

A numerical relativistic model of a massive particle in orbit near a Schwarzschild black hole

Nigel T. Bishop,¹ Roberto Gómez,^{2,3} Sascha Husa,⁴ Luis Lehner,^{5,6} and Jeffrey Winicour^{4,3}

¹*Department of Mathematics, Applied Mathematics and Astronomy,
University of South Africa, P.O. Box 392, Pretoria 0003, South Africa*

²*Pittsburgh Supercomputing Center, 4400 Fifth Ave., Pittsburgh, Pennsylvania 15213, U.S.A.*

³*Department of Physics and Astronomy, University of Pittsburgh, Pittsburgh, PA 15260, U.S.A.*

⁴*Max-Planck-Institut für Gravitationsphysik, Albert-Einstein-Institut, Am Mühlenberg 1, D-14476, Golm, Germany*

⁵*Department of Physics and Astronomy, Louisiana State University, Baton Rouge, LA 70810, U.S.A.*

⁶*University of British Columbia, Vancouver, BC, Canada V6T-1Z1*

(Dated: January 16, 2003, Version 2.4, REVTeX 4)

We present a method for computing the evolution of a spacetime containing a massive particle and a black hole. The essential idea is that the gravitational field is evolved using full numerical relativity, with the particle generating a non-zero source term in the Einstein equations. The matter fields are not evolved by hydrodynamic equations. Instead the particle is treated as a rigid body whose center follows a geodesic. The necessary theoretical framework is developed and then implemented in a computer code that uses the null-cone, or characteristic, formulation of numerical relativity. The performance of the code is illustrated in test runs, including a complete orbit (near $r = 9M$) of a Schwarzschild black hole.

PACS numbers: 04.25.Dm, 04.20.Ex, 04.30.Db, 95.30.Lz

I. INTRODUCTION

This paper is concerned with the evolution of a spacetime containing a small object in orbit near a black hole, the objective being to compute the motion of the object and the emitted gravitational radiation. The techniques normally used for tackling this type of problem are related to the treatment of ‘radiation-reaction’ problems. The small object is treated as a particle evolving on a fixed background spacetime with its self-force somehow taken into account. There are a number of approaches concerning the implementation of the self-force – for example [1, 2, 3, 4, 5, 6, 7, 8, 9]. An alternative approach that could be used is full numerical relativity including computational relativistic hydrodynamics (see for example [10, 11, 12, 13, 14, 15], and for a review [16]); but to our knowledge, such simulations have not been performed for the extreme mass ratios considered in this paper.

The approach developed here uses full numerical relativity but with the hydrodynamic aspect greatly simplified, and can be described as a *massive particle method*. We use full numerical relativity for the evolution of the gravitational field (including a non-zero stress energy tensor as source). The matter fields are not evolved by relativistic hydrodynamics but rather the object is treated as a rigid body whose center is evolved by the geodesic equation. This approach avoids the intricacies and computational expense of relativistic hydrodynamics.

Of course, there are limitations to the particle approach: it can only be applied in situations in which the internal hydrodynamics of the material object are unimportant, and in which the assumption of rigidity is reasonable. For example, one would certainly need full numerical relativity and relativistic hydrodynamics in situations in which the object is expected to be tidally

disrupted. On the other hand, if tidal effects are small (in a sense that will be made precise), then the particle model should provide a good description of the physics.

The bounds of the domain of applicability of the particle method have not been investigated in any systematic way. However, heuristically, as well as from the example runs presented later, the method should be applicable under appropriate restrictions, e.g. when the mass m of the particle is $m \leq 10^{-5}M$ (where M is the mass of the black hole) and when the dimension of the particle is small enough that it not be tidally disrupted. Thus, we expect the particle method to be applicable in astrophysical situations involving the inspiral and capture of a neutron star or white dwarf by a galactic black hole (with M about $10^6 M_\odot$). On the other hand, it is difficult to see how the method could be used for a stellar remnant black hole (with M about $10 M_\odot$) – any object with small enough m/M would have too large a diameter. Thus the method is expected to make predictions concerning gravitational radiation that will be relevant to observations by LISA [17], rather than to observations by LIGO or other earth based detectors.

The results presented here use a characteristic gravity code [18, 19]. However, there is no reason to restrict the particle method to the characteristic approach. The method should also be applicable within Cauchy formulations of numerical relativity.

We develop and investigate two different theoretical models of a massive particle: the δ -function and the polytropic models. Both models have limitations, but, in the present implementation, the polytropic model performs better, giving smoother results and, in particular, exhibiting convergence with grid-refinement (as described in Sec. V A). The δ -function model cannot be convergent, since the matter density depends on the grid

size. Nevertheless, there are useful reasons for considering the δ -function model, as discussed in Sec. VI.

The purpose of this paper is to introduce the particle method. We also give some example runs exhibiting inspiral and a plunge to the black hole. These runs demonstrate the potential of the method, and are not presented as an accurate description of the physics. Of course, validated physical results are the goal of this project but, as discussed in sec. VI, much more computational testing is needed before the goal can be attained.

We begin by summarizing previous results on the characteristic formulation of numerical relativity in Sec. II. Then issues concerning the theoretical framework of a massive particle, including the two models used here, are discussed in Sec. III. Section IV presents, in detail, the computational algorithms. Tests of the code and other example runs are given in Sec. V.

II. SUMMARY OF PREVIOUS RESULTS, AND NOTATION

The formalism for the numerical evolution of Einstein's equations, in null cone coordinates, is well known [18, 20, 21] (see also [22, 23, 24, 25, 26]). For the sake of completeness, we give here a summary of the formalism, including some of the necessary equations. The version of the gravity code being used here is fully described in [19].

We use coordinates based upon a family of outgoing null hypersurfaces. We let u label these hypersurfaces, x^A ($A = 2, 3$), label the null rays and r be a surface area coordinate. In the resulting $x^\alpha = (u, r, x^A)$ coordinates, the metric takes the Bondi-Sachs form [25, 27]

$$ds^2 = - \left(e^{2\beta} \left(1 + \frac{W}{r} \right) - r^2 h_{AB} U^A U^B \right) du^2 - 2e^{2\beta} du dr - 2r^2 h_{AB} U^B dx^A + r^2 h_{AB} dx^A dx^B, \quad (2.1)$$

where $h^{AB} h_{BC} = \delta_C^A$ and $\det(h_{AB}) = \det(q_{AB})$, with q_{AB} a unit sphere metric. We work in stereographic coordinates $x^A = (q, p)$ for which the unit sphere metric is

$$q_{AB} dx^A dx^B = \frac{4}{F^2} (dq^2 + dp^2), \quad \text{where } F = 1 + q^2 + p^2. \quad (2.2)$$

(In previous notation we used $P = 1 + q^2 + p^2$. Here we change notation to F because P now represents pressure, which we cannot denote by p because that is a stereographic coordinate). We also introduce a complex dyad $q^A = \frac{F}{2}(1, i)$ with $i = \sqrt{-1}$. For an arbitrary Bondi-Sachs metric, h_{AB} can then be represented by its dyad component

$$J = h_{AB} q^A q^B / 2, \quad (2.3)$$

with the spherically symmetric case characterized by $J = 0$. We introduce the (complex differential) eth operators $\bar{\delta}$ and δ (see [28] for full details), as well as a number of

auxiliary variables $K = h_{AB} q^A \bar{q}^B / 2$, $U = U^A q_A$, $Q_A = r^2 e^{-2\beta} h_{AB} U_{,r}^B$, $Q = Q_A q^A$, $B = \bar{\delta} \beta$, $\nu = \bar{\delta} J$ and $k = \bar{\delta} K$.

The Einstein equations decompose into hypersurface equations, evolution equations and conservation laws. The hypersurface equations form a hierarchical set for $\nu_{,r}$, $k_{,r}$, $\beta_{,r}$, $B_{,r}$, $(r^2 Q)_{,r}$, $U_{,r}$ and $W_{,r}$; and the evolution equation is an expression for $(rJ)_{,ur}$. The explicit form of the equations is given in [19] in the vacuum case; and the matter source terms are stated in [29], except that the matter source term in Eq. [29]–(31) is incorrect and that equation should read

$$2(rJ)_{,ur} - \left((1 + r^{-1}W)(rJ)_{,r} \right)_{,r} = -r^{-1} (r^2 \bar{\delta} U)_{,r} + 2r^{-1} e^{\beta} \bar{\delta}^2 e^{\beta} - (r^{-1}W)_{,r} J + N_J + \frac{4e^{2\beta} \pi(\rho + P)}{r} ((J\bar{V}_{ang} - KV_{ang})^2 + V_{ang}^2), \quad (2.4)$$

where $V_{ang} = v_A q^A$ [29], with v_i the velocity of the mass m particle, ρ and P its density and pressure and N_J defined in [18] and [19]. The remaining Einstein equations reduce to conservation conditions which need only be satisfied on the inner boundary, which are automatically satisfied here because the boundary has a simple Schwarzschild geometry.

The null cone problem is normally formulated in the region of spacetime between a timelike or null worldtube Γ and \mathcal{I}^+ . We represent \mathcal{I}^+ on a finite grid by using a compactified radial coordinate $x = r/(1+r)$. The numerical grid is regular in (x, q, p) and consists of two patches (north and south), each containing $n_x n_q n_p$ grid-points. The x -grid covers the range $[0.5, 1]$. Each angular grid patch extends two grid-points beyond the domain $(q, p) \in [-q_s, q_s] \times [-q_s, q_s]$, with $q_s \geq 1$. Thus there is an overlap region at the equator with larger overlap for larger q_s .

We denote the Bondi-Sachs metric (2.1) by $g_{\alpha\beta}$ and the background metric ($g_{\alpha\beta}$ with $J = U = \beta = 0$, $W = -2M/r$) by $g_{[M]\alpha\beta}$. The mass M of the black hole is normally scaled to $M = 1$ in simulations.

III. THEORETICAL FRAMEWORK

We have developed two different particle models with rather different conceptual frameworks but implemented with very similar numerical codes. This section describes each of the two frameworks, as well as some other theoretical issues.

A. The δ -function model

At the analytic level, a point particle of mass m at position $z^\alpha = (u, z^i) = (u, r, z^A)$ has density ρ and 4-velocity v^α satisfying

$$\rho \sqrt{-g} v^\alpha = m \delta(x^i - z^i), \quad (3.1)$$

where $\int \delta(x^i - z^i) drdqdp = 1$. We model the δ -function on the grid by assigning weights w to each grid point in a stencil surrounding the particle. In terms of a test function ϕ , this requires

$$\phi(z^i) = \sum_I \phi_I w_I \Delta_V \quad (3.2)$$

where \sum_I is a sum over a stencil I of grid points surrounding the particle position z^i and Δ_V is the coordinate 3-volume of the stencil I . We determine the weights w_I representing the δ -function by choosing a set of test functions, e.g. for the stencil of eight points determined by the cell surrounding the particle we choose

$$\begin{aligned} \phi = & a + a_i(x^i - z^i) + a_{ij}(x^i - z^i)(x^j - z^j) \\ & + a_{ijk}(x^i - z^i)(x^j - z^j)(x^k - z^k), \end{aligned} \quad (3.3)$$

where $i \neq j \neq k$ so that the a 's constitute eight arbitrary coefficients. This then gives 8 simultaneous equations to solve for the w_I .

The matter satisfies the exact conservation law $\nabla_\alpha(\rho v^\alpha) = 0$. This is automatically satisfied, in integral form, by the above grid representation of the density. In this way the time dependence of ρ is not free but determined by the time dependence of the metric and 4-velocity.

B. The polytropic model

The polytropic model treats the particle as an object of fixed size described by the worldline of its center $z^i(u)$. The simplest model of a polytrope, which will be used here, is for the case with index $n = 1$. Then the density ρ and the pressure P are given by [30]

$$\rho = \frac{m \sin \frac{R\pi}{R_*}}{4RR_*^2}, \quad P = \frac{2R_*^2 \rho^2}{\pi}, \quad (3.4)$$

for $R \leq R_*$, and $\rho = P = 0$ for $R > R_*$, where R_* is the radius of the polytrope and R is a distance from its center, defined as follows. At a point $x^\alpha = (u, x^i)$, we first define the displacement vector ϵ^α relative to the polytrope's center

$$\epsilon^u = 0, \quad \epsilon^i = x^i - z^i(u). \quad (3.5)$$

The projection of ϵ^α into the hypersurface orthogonal to the worldline at time u is

$$R_\alpha = (g_{\alpha\beta} + v_\alpha v_\beta) \epsilon^\beta, \quad (3.6)$$

with $g_{\alpha\beta}$ evaluated at x^α , and v_α evaluated at time u . Then R is defined as the magnitude of the orthogonal displacement,

$$R = \sqrt{g^{\alpha\beta} R_\alpha R_\beta}. \quad (3.7)$$

As usual, the perfect fluid condition is used to set the stress-energy tensor $T_{\alpha\beta}$.

The polytropic model has the advantage over the δ -function model of allowing convergence tests (see Sec. V A) but it has the disadvantage of being only an approximate model in the following sense. Equation (3.4) is exact only for an isolated sphere in equilibrium in Newtonian theory. In general relativity it is a good approximation only if $m \ll R_*$. Furthermore, in the field of a black hole, the polytrope would not preserve its spherical shape but would become tidally distorted. Both these approximations introduce the same type of error - the polytrope's motion is treated as though it were a rigid body but, for the purpose of determining its gravitational field, its stress-energy tensor $T_{\alpha\beta}$ is modeled as a perfect fluid. Thus, in the approximation being made, there are additional contributions to $T_{\alpha\beta}$ that are being ignored. This is discussed further in Sec. VI.

C. Particle evolution from approximate conservation laws

The motion of a test particle in a background Schwarzschild geometry satisfies certain conservation laws. For a particle with mass $0 < m \ll M$, these conservation laws are not satisfied but they can be useful because they represent quantities that change very slowly. Our strategy is to use the Schwarzschild conservation laws to define approximately conserved quantities, and then compute the evolution of those quantities in the general case. In this process, all background terms cancel out and we are left with expressions involving only small quantities.

For the case of a test particle in the Schwarzschild geometry there is a reflection symmetry plane, the plane of the orbit. Thus the normalized 4-velocity is completely determined by its components $T^\alpha v_\alpha = v_u$ and $\Phi^\alpha v_\alpha = v_\phi$, where T^α and Φ^α are the Killing vectors of the Schwarzschild background and v_ϕ is a velocity component with respect to (u, r, θ, ϕ) null-spherical coordinates. In the general case, v_u and v_ϕ are approximately conserved.

We neglect internal forces and start with the conservation law $\nabla_\beta(\rho v^\alpha v^\beta) = 0$ to obtain

$$\nabla_\beta(\xi^\alpha \rho v_\alpha v^\beta) = \rho v_\alpha v_\beta \nabla^\alpha \xi^\beta = -\frac{1}{2} \rho v_\alpha v_\beta \mathcal{L}_\xi g^{\alpha\beta}, \quad (3.8)$$

where ξ^α represents T^α or Φ^α . Integration over a worldtube surrounding the particle between times u and $u+du$ then gives

$$m \frac{d(\xi^\alpha v_\alpha)}{du} = -\frac{m}{2v^u} v_\alpha v_\beta [\mathcal{L}_\xi g^{\alpha\beta}]_c \quad (3.9)$$

where $[\mathcal{L}_\xi g^{\alpha\beta}]_c$ is centered about the location of the particle. Partly because of the stereographic coordinates being used, the implementation of Eq. (3.9) is quite technical (see Sec. IV D for details).

D. Background metric

In the δ -function model, it is necessary to renormalize the metric so as to avoid infinities in the equations of motion. The metric occurs through the normalization of the 4-velocity v_α and the raising of indices. We take the components (v_r, v_A) to be basic since they represent the pullback of the 4-velocity to the null hypersurface. We renormalize the other components by using the background metric $g_{[M]\alpha\beta}$ to raise indices and to normalize the 4-velocity. This avoids the problem of an infinite self-potential energy of the particle and is in keeping with the principle that the energy of the particle only depends on its velocity and position in the Schwarzschild field.

In the polytropic model, the above renormalization is not necessary, but it is convenient and is justified by the same argument. However, in this case, the code can be run either with or without such metric renormalization.

It should be emphasized that this renormalization, or use of $g_{[M]\alpha\beta}$ rather than $g_{\alpha\beta}$, applies only to the *undifferentiated* metric. Metric derivatives that occur in the particle equations of motion are computed using the full metric $g_{\alpha\beta}$ – otherwise radiation reaction could not be included and we would simply be computing the motion of a test particle in the Schwarzschild geometry. Of course, it is the full metric which is evolved by the characteristic algorithm.

E. Caustics

The characteristic evolution code breaks down if caustics develop, which render the null coordinate system employed singular. A rough estimate can be readily obtained by employing the well-known condition for the deflection of light by a massive body such as the Sun. We find as an approximate condition for caustics not to form that

$$\frac{r_p^2}{4m} > r, \quad (3.10)$$

where in the polytropic model $r_p = R_*$ and in the δ -function model r_p is half of the proper length of an angular edge of the grid cell containing the particle.

IV. COMPUTATIONAL METHOD

A. Overview

The particle method constitutes a complete evolution of the matter and gravity fields. As discussed in section III, the particle can be modeled as either a δ -function or a polytrope. In the δ -function model, the density is distributed among the 8 grid points of the cell containing the particle, according to the procedure described in Sec. III A. In the polytrope model, the density and pressure are allocated to each grid-point at which $\rho \neq 0$; in

this case, the polytrope spans several grid-cells. In both models, the particle's density, pressure (if non-zero) and 3-velocity v_i are used to construct the right hand side of the Einstein equations, which are then used to evolve the gravitational field as described in section II.

The gravitational field affects the motion of the particle. The 3-velocity v_i is evolved by using the geodesic equation in the form

$$\frac{dv_i}{du} = \frac{\Gamma_{\alpha i \gamma} v_\delta v_\epsilon g^{\alpha\delta} g^{\gamma\epsilon}}{v^u}; \quad (4.1)$$

and the particle's position is evolved by

$$\frac{dz^i}{du} = \frac{v^i}{v^u}. \quad (4.2)$$

The setting of initial data is described in Sec. IV C below. The worldtube Γ at $r = 2M$ is the (past) horizon of a Schwarzschild black hole of mass M . Thus the boundary data on Γ has the simple analytic form [29]

$$J = \nu = k = \beta = B = U = Q = 0, \quad W = -2M. \quad (4.3)$$

B. Details of the computational algorithms

The iterative evolution algorithm proceeds as follows:

1. Start at time $u = u^{(n)}$. The gravitational field $g_{\alpha\beta}^{(n-1)}$ is known over the whole grid and the boundary data supplies $g_{\alpha\beta}^{(n)}$ in a neighborhood of $r = 2M$. The particle's position $z^{i(n)}$ and velocity $v_i^{(n)}$ are also known.
2. Determine the grid-cell $G_P^{(n)}$ containing the point $z^{i(n)}$; i.e., determine a_i such that

$$\begin{aligned} r^{(a_1)} &< z^{1(n)} < r^{(a_1+1)}, \\ q^{(a_2)} &< z^{2(n)} < q^{(a_2+1)}, \\ p^{(a_3)} &< z^{3(n)} < p^{(a_3+1)}. \end{aligned} \quad (4.4)$$

This is done on both north and south patches, although if the particle is not in the equatorial overlap region there will be a solution for only one of the patches. We define

$$\begin{aligned} \Delta^{i(n)} &= x^{a_i+1} - x^{a_i}, & \delta_0^{i(n)} &= x^{a_i+1} - z^{i(n)}, \\ & & \delta_1^{i(n)} &= z^{i(n)} - x^{a_i} \end{aligned} \quad (4.5)$$

and we define the weights representing the δ -function at the eight grid-points at the corners of $G_P^{(n)}$ by

$$w(x^{a_i+e_i}) = \frac{\delta_{e_1}^{1(n)} \delta_{e_2}^{2(n)} \delta_{e_3}^{3(n)}}{\Delta^{1(n)} \Delta^{2(n)} \Delta^{3(n)}}, \quad (4.6)$$

where $e_i = \{0, 1\}$. These weights satisfy the requirements stated in section III A.

3. Next, we set the density and pressure. In general, this needs to be done on both north and south patches.

- In the δ -function model, the pressure is zero and there is a non-zero density only at the corners of the grid-cell $G_P^{(n)}$. The density is given by

$$\rho(x^{a_i+e_i}) = -mw(x^{a_i+e_i}) \frac{F^2}{4v_r r^2 \Delta_V} \frac{dx}{dr}. \quad (4.7)$$

where Δ_V is the coordinate-volume of a grid-cell, i.e. $\Delta_V = \Delta_x \Delta_q \Delta_p$; and where F , r and dx/dr are evaluated at $z^{i(n)}$.

- In the polytropic model, the density at the grid-point x^i is set by means of Eqs. (3.4)-(3.7); then the pressure P is set.
4. The Einstein equations are now integrated to find the metric $g_{\alpha\beta}^{(n)}$. The source terms are given in [29] (where, as already noted, Eq. [29]-(31) should be replaced by Eq. (2.4)).
 5. The formula $g^{\alpha\beta} v_\alpha v_\beta = -1$ is used to find $v_u^{(n)}$; the metric $g^{\alpha\beta}$ is known at the required grid-points and its value at the particle position $z^{i(n)}$ is found by taking a weighted average using the weights found in step 3 above.
 6. The formula $v^\alpha = g^{\alpha\beta} v_\beta$ is used to find $v^{\alpha(n)}$, again using the weighted average to find $g^{\alpha\beta}$.
 7. Equation (4.2) is now used to find $z^{i(n+1)}$. On the first time-step, this is done by the Euler method and, on subsequent time steps, by the 3-point Adams-Bashforth method, i.e.

$$z^{(n+1)} = z^{(n)} + \frac{\Delta u}{2} \left(3 \frac{dz^{(n)}}{du} - \frac{dz^{(n-1)}}{du} \right) \quad (4.8)$$

8. We now find $v_i^{(n+1)}$. The right hand side of Eq. (4.1) is evaluated at $z^{i(n)}$ by, as usual, finding the value at the grid-points and taking a weighted average using the weights found in step 3 above. The terms in Eq. (4.1) are quite complicated and were found using a Maple script, which was also used to generate Fortran code. Details are given in an Appendix. The numerical evolution method is the same as used in step 7.

C. Setting the initial data

In the example runs presented below, the initial gravitational content is prescribed by setting $J = 0$. The code is then evolved for a pre-determined time u_S , during which the gravitational field produces strong accelerations. However during this time the particle's velocity and position are not updated. The idea here is that the gravitational field should have relaxed to the correct form by the time u_S when the particle is allowed to move. The optimal value of u_S has not been determined in a systematic way, but rather runs similar to those in Sec. V D and

V E indicate that gravitational initialization effects are dissipating by $u_S \approx 2$; and so, including a safety factor, we normally take $u_S = 5$. It is also possible to set the initial data J by a Newtonian limit condition [21, 31, 32], the computational implementation of which will be discussed elsewhere.

The code requires the initial velocity as a 1-form v_i but a physical description normally specifies the tangent vector v^i . For example, a particle in a circular orbit would have

$$v^r = 0, \quad (v^p)^2 + (v^q)^2 = \frac{F^2 M}{4r^2(r - 3M)}. \quad (4.9)$$

Suppose that we are given v^i rather than v_i . Initially, when only the background metric is known, v_i is constructed from v^i using

$$g_{[M]\alpha\beta} v^\alpha v^\beta = -1 \quad (4.10)$$

to first determine v^u ; then $v_i = g_{[M]i\alpha} v^\alpha$.

If the background option is being used (see Sec. III D), the setting of v_i is complete; if not then, while $u < u_S$, the code uses the fact that v^α is found at each time step to determine a value of v_r such that $v^r = 0$ by an iterative algorithm. Explicitly, we use the secant algorithm

$$v_{r(a+1)} = v_{r(a)} - v_{r(a)}^r f_S \frac{v_{r(a)} - v_{r(a-1)}}{v_{r(a)}^r - v_{r(a-1)}^r}, \quad (4.11)$$

where a is the iteration number and f_S is a factor (which is 1 in the standard algorithm) that may need to be set to 0.2 or smaller for stable convergence – the difficulty here is that we are solving $v^r(v_r) = 0$ not as a simple algebraic equation but as an equation whose coefficients change as the metric relaxes.

D. Implementation of the approximate conservation laws

The theoretical basis for approximate angular momentum and energy conservation was discussed in Sec. III C. We now present details of how this is implemented for (1) the angular momentum in an equatorial orbit, (2) the angular momentum in a polar orbit, and (3) the energy. The code is written so that all of these approximate conservation laws may be used, or not, simply by changing input parameter switches.

Angular velocity in an equatorial orbit

The angular momentum per unit mass

$$h = qv_p - pv_q \quad (4.12)$$

is approximately conserved. In terms of proper time τ along the particle's trajectory,

$$\frac{dh}{d\tau} = v^q v_p + q \frac{dv_p}{d\tau} - v^p v_q - p \frac{dv_q}{d\tau}. \quad (4.13)$$

Now, Eq. (4.1) takes the form

$$\frac{d}{d\tau}v_A = -\frac{z^A}{r^2}((v_p)^2 + (v_q)^2) + E_A, \quad A = (q, p), \quad (4.14)$$

where the E_A contain only small quantities. We also introduce $\mu^i = (g^{i\alpha} - g_{[M]}^{i\alpha})v_\alpha$, which represents the difference between raising an index by the full or background metric. Thus,

$$v^A = \mu^A + \frac{v_A}{r^2}. \quad (4.15)$$

Of course, $\mu^i = 0$ if the background option is in use. Combining Eqs. (4.13), (4.14) and (4.15), we obtain

$$\frac{dh}{d\tau} = \mu^q v_p - \mu^p v_q + qE_p - pE_q, \quad (4.16)$$

which is implemented in the code. We extract v_A from the evolved value of h . This is done by using the constraint that the particle is on the equator, $q^2 + p^2 = 1$. Thus $qv^q + pv^p = 0$ so that

$$q\left(\mu^q + \frac{v_q}{r^2}\right) + p\left(\mu^p + \frac{v_p}{r^2}\right) = 0. \quad (4.17)$$

Combining Eqs. (4.12) and (4.17), we find

$$\begin{aligned} v_q &= -ph - r^2 q(q\mu^q + p\mu^p) \\ v_p &= qh - r^2 p(q\mu^q + p\mu^p), \end{aligned} \quad (4.18)$$

which is implemented in the code. Furthermore, the particle is constrained to follow the equator exactly, and so the particle's position is corrected according to $z^A \rightarrow z^A f_e$ with

$$f_e = \sqrt{\frac{1}{q^2 + p^2}}. \quad (4.19)$$

Angular velocity in a polar orbit

In the case of polar motion, simplified here to the case $p = 0$, the equations analogous to Eqs. (4.12), (4.16) and (4.18) are

$$h = \frac{Fv_q}{2}, \quad \frac{dh}{d\tau} = \frac{FA_q}{2} + qv_q\mu^q, \quad v_q = \frac{2h}{F}. \quad (4.20)$$

The energy

The energy per unit mass v_{uS} is conserved along a geodesic in the Schwarzschild background. In this case

$$v_{uS} = \frac{h^2 + r^2 + v_r^2(r^2 - 2Mr)}{2v_r r^2}. \quad (4.21)$$

We take v_{uS} , as defined above, to be an approximately conserved quantity. From Eq. (4.1),

$$\frac{d}{d\tau}v_r = -\frac{h^2}{r^3} - \frac{v_r^2 M}{r^2} + E_1. \quad (4.22)$$

Using

$$\frac{dr}{d\tau} = v^r = -v_{uS} + \left(1 - \frac{2M}{r}\right)v_r + \mu^r, \quad (4.23)$$

differentiation of Eq. (4.21) leads to

$$\begin{aligned} \frac{d}{d\tau}v_{uS} &= \left(2h\frac{dh}{d\tau}rv_r + 2v_r^3Mr\mu^r - 2h^2v_r\mu^r \right. \\ &\quad \left. + E_1(r^3v_r^2 - r^3 - 2Mr^2v_r^2 - h^2r)\right)\frac{1}{2r^3v_r^2}. \end{aligned} \quad (4.24)$$

There is an option in the code to evolve v_{uS} by Eq. (4.24). In this case, we extract v_r from the value of v_{uS} . This is done by rewriting Eq. (4.21) as a quadratic in v_r . We find

$$v_r = \frac{v_{uS} \pm \sqrt{v_{uS}^2 - \left(1 - \frac{2M}{r}\right)\left(1 + \frac{h^2}{r^2}\right)}}{\left(1 - \frac{2M}{r}\right)}. \quad (4.25)$$

When the code is evolving v_{uS} by Eq. (4.24), at each time step it also evolves v_r in the usual way. The \pm in Eq. (4.25) is chosen so that the result for v_r is closest to the directly evolved value; further, if the square root in Eq. (4.25) is less than some threshold, or imaginary, the directly evolved value of v_r is not corrected. For a circular orbit of the Schwarzschild background, the square root is exactly zero, and therefore it is difficult to use this option when evolving a circular orbit.

E. Other features of the code

- The only Bondi-Sachs metric variable that is non-zero in the background metric is W . The code treats W as the sum of the background analytic part (W_{an}) plus a correction (W_{num}). The values of W_{an} and its derivatives are found exactly, and finite differencing is applied only to the part W_{num} . In effect, this also applies to the other metric variables, because their background analytic parts are zero.
- There is an option in the code to use an enlarged stencil in the computation of the (centered) finite differences used in $\Gamma_{\alpha i \gamma}$ in Eq. (4.1). The evolution of the gravitational field is not affected. More precisely, use of this option means that

$$\frac{df(x_i)}{dx} \approx \frac{f(x_{i+i_s}) - f(x_{i-i_s})}{2i_s \Delta_x} \quad (4.26)$$

with $i_s > 1$. This option uses grid-points away from the particle in computing derivatives, and thus smooths them. It is used in the δ -function model with $i_s = 3$, but not in the polytropic model. The issue is discussed further in Sec. VI.

V. COMPUTATIONAL TESTS AND RESULTS

A. Convergence

The convergence testing was limited to a measurement of various accelerations on the initial null cone, and we have not investigated convergence behavior after a fixed time. The difficulty with convergence testing over an extended time period is the computational resources required for the finest grid, and we defer such testing to future work (see Sec. VI)

The tests were made with the particle initialized at $r = 9$ at the north pole with $v^p = 0$ and v^q set to the value for a circular orbit. The particle mass was $m = 10^{-4}$. The particle was always allowed to move, i.e. $u_S = 0$. The particle velocity was updated directly, and not via approximate conservation laws. The overlap between north and south patches was minimal ($q_s = 1.0$). The polytropic model was used with $R_* = 5.0$. The following quantities, all of which are rates of change, were determined on the initial null cone: $\|J_{,u}\|_\infty$, $h_{,u}$, $v_{u,u}$, $v_{r,\tau}$ and $v_{q,\tau}$. The quantities involving u -derivatives were found by evolving the code for one time-step and then applying the formula $Q_{,u} = (Q_1 - Q_0)/\Delta u$; the quantities involving τ -derivatives are found directly by the code using data only on the initial null cone.

The following grids were used: (a) coarse, $n_x = 41$, $n_q = n_p = 25$; (b) medium $n_x = 81$, $n_q = n_p = 45$; and (c) fine, $n_x = 161$, $n_q = n_p = 85$. In the different grids, Δ_x and $\Delta_q = \Delta_p$ scale as 4:2:1. The (single) time-step was $\Delta u = 10^{-5}$, which, for all grids, is much smaller than the spatial discretization. Assuming that a quantity Q behaves as $Q = a + b\Delta^n$, it is straightforward to show that

$$n = \log_2 \frac{Q_c - Q_m}{Q_m - Q_f} \quad (5.1)$$

where Q_c , Q_m and Q_f refer to the computed values of Q using the coarse, medium and fine grids, respectively.

Our results are stated in Table I: it is clear that, on the initial null cone, the polytropic model is convergent with the order n at least 1.59.

B. Gravitational radiation

Unfortunately, it is not possible to present any results on gravitational radiation output. The module used in

TABLE I: Convergence of the Polytropic model

	Coarse	Medium	Fine	n
$\ J_{,u}\ _\infty$	0.4346×10^{-2}	0.4441×10^{-2}	0.4460×10^{-2}	2.28
$h_{,u}$	-0.7377×10^{-2}	-0.3436×10^{-2}	-0.2129×10^{-2}	1.59
$v_{u,u}$	0.2732×10^{-4}	0.1273×10^{-4}	0.0789×10^{-4}	1.59
$v_{r,\tau}$	-0.5050×10^{-3}	-0.5455×10^{-3}	-0.5564×10^{-3}	1.9
$v_{q,\tau}$	-1.8069×10^{-3}	-0.8416×10^{-3}	-0.5215×10^{-3}	1.59

this code for calculating the news [18] was originally developed and tested under conditions in which the fields are well resolved at \mathcal{I}^+ , which is not the case here. For particle applications, the module produces questionable results, such as significant radiation when the gravitational field is static. Improvements in the accuracy of the news module have recently been made [33] but they have not been tested in the present context. Thus it is not yet known whether reliable radiation measurements for a particle source can be made or if perhaps further algorithmic refinements will be needed. Results will be reported elsewhere after the necessary development and testing.

C. Increase m until caustics form

A simple test of the code is to increase the particle mass m until the code crashes due to the formation of a caustic, which is indicated by the metric variable $\beta \rightarrow \infty$. The following test was performed using the δ -function model with initial velocity $v^i = 0$, initial position $r = 9$ at the north pole, and discretization $n_x = 41$ and $n_q = n_p = 25$. Equation (3.10) indicates that the critical value of m is 2.25×10^{-2} . In trial runs, the code behaves properly with $m = 10^{-3}$ but crashes when $m = 10^{-2}$.

D. Whole orbit

This test was performed for both the δ -function and polytropic models. The particle was initialized at $r = 9$, $q = 0$, $p = 1$ with an initial velocity in the q -direction of magnitude such that, in the test particle limit, the orbit would be exactly circular. The mass of the particle was taken as $m = 10^{-6}$ and the size taken as $R_* = 3.0$ in the polytropic model. The grid discretization was $n_x = 121$ and $n_q = n_p = 35$. The time step was $dt = 8.3333 \times 10^{-3}$. The code was run with angular grid patch overlap set by $q_s = 1.2$; and with no particle motion until $u_S = 5.0$. In order to achieve a complete orbit, the computation was run until $u = 175$, which required 21,000 time-steps. The background option (see Sec. III D) was used. The angular momentum h was evolved but the energy v_u was not evolved.

An important requirement was that the simulations should complete in a reasonable time, and thus there was a limit on the number of grid-points that could be used. Further, in the polytropic model, the requirement that the polytrope should be resolvable places a lower limit on R_* . The run was performed for illustrative purposes and, in the polytropic model case, is not physical because a polytrope with the parameters used here would be tidally disrupted.

The results of the computation are shown in Figs. 1 to 4 for the polytropic and δ -function models. In both cases, the particle inspirals, losing energy and angular momentum, but the effect is much smoother and smaller

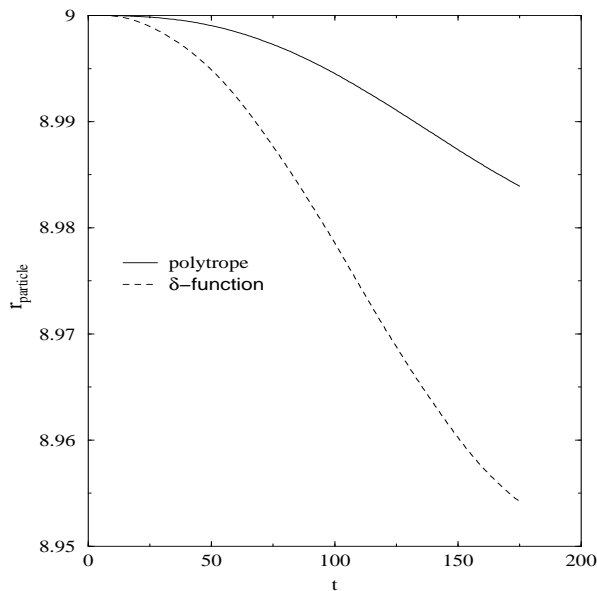


FIG. 1: r -coordinate for the polytropic (solid line) and δ -function model (dotted line) for a complete orbit.

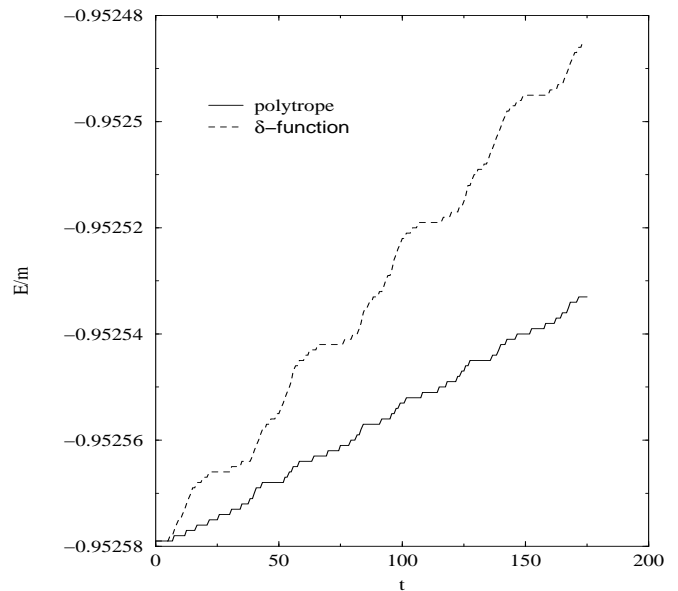


FIG. 3: Energy per unit particle mass for the polytropic (solid line) and δ -function model (dotted line) for a complete orbit.

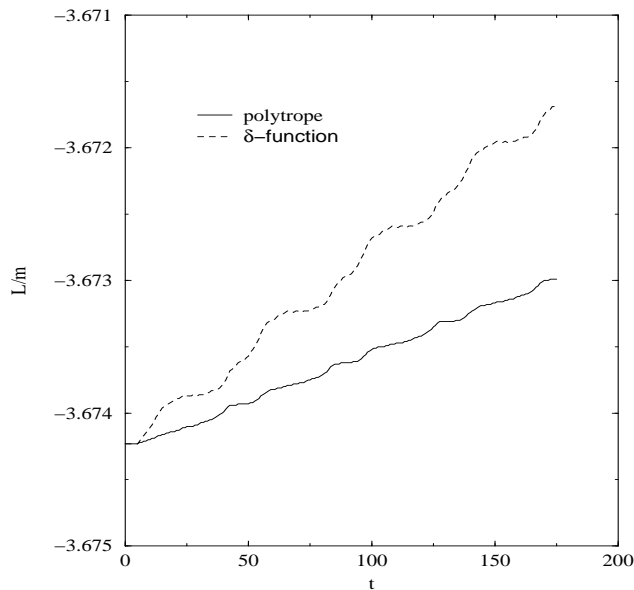


FIG. 2: Angular momentum per unit particle mass for the polytropic (solid line) and δ -function model (dotted line) for a complete orbit.

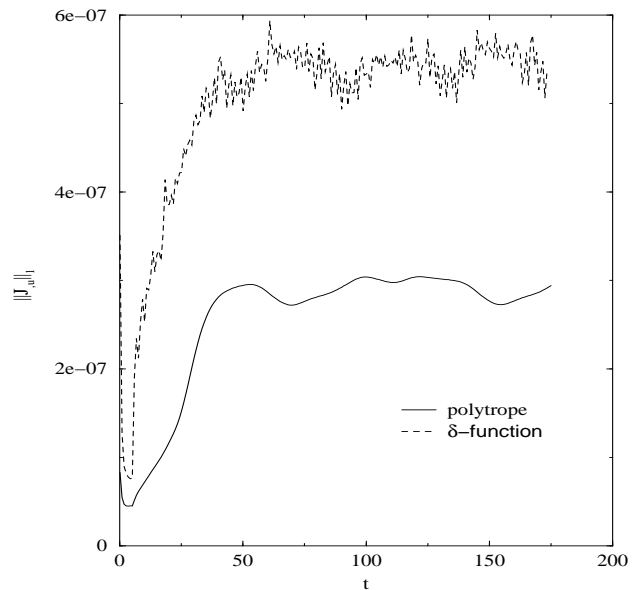


FIG. 4: $L-1$ norm, $\|J_{,u}\|_1$ for the polytropic (solid line) and δ -function model (dotted line) for a complete orbit.

in the polytropic case. Figure 4 shows the time development of the L_1 norm of $J_{,u}$, which measures the rate of change of the gravitational field. Again, the polytropic model exhibits smoother and smaller behavior.

E. Capture of particle by the black hole

The code parameters were the same as for the previous test, except that in the polytropic model $R_* = 2.0$, and the particle was initialized at $r = 6$ near the ISCO. The

purpose of the test was to see how the code behaves as the particle approaches the event horizon at $r = 2$. In order to shorten the inspiral time the particle was given a small inward radial velocity ($v^r = -0.01$), and the angular velocity was set to that for a circular orbit in the test particle limit ($v^{\theta} = 0.09622504486$, $v^{\phi} = 0$).

In the coordinates being used, as $r \rightarrow 2$ the evolution variable $v_r \rightarrow \infty$. Thus, because of this coordinate effect, we expect the code to crash at some value of r just greater than 2. The results of the computation (in the polytropic case) are shown in Figs. 5 to 8. The particle inspirals from $u = u_S (= 5)$ until the code crashes at $u = 186.666$ with the particle at $r = 2.00077$ and $|v_r| \approx 5,000$. The particle completed just over two complete revolutions, i.e. its angular position changed by just over 4π radians during the evolution. The particle crossed $r = 2.1$ at $u = 167$, $r = 2.01$ at $u = 176$ and $r = 2.001$ at $u = 185$; thus demonstrating a freezing of radial position, as expected due to the redshift inherent in the u -coordinate. Throughout the computation, the position of the particle is remarkably smooth. The particle loses energy and angular momentum at a fairly constant rate, until about $u = 150$, $r = 3.2$. Further, the activity of the gravitational field (as measured by $\|J_{,u}\|$) starts to grow rapidly at this time. We have not analyzed the cause of this effect. As in the whole orbit computation, the performance of the δ -function model was much less smooth than that of the polytropic model.

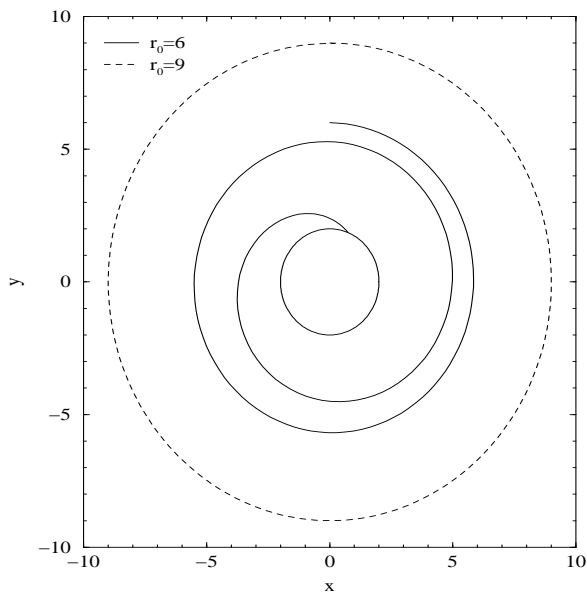


FIG. 5: The orbit traced by a particle (polytropic model), initially at $r = 6$, as it is captured by a black hole (solid line). Overlaid in the figure is the orbit traced by a particle initially at $r = 9$ (dotted line). The central circle indicates the location of the horizon ($r = 2$).

In this case, the δ -function particle reached $r = 2.006$ at $u = 174$ when the code crashed.

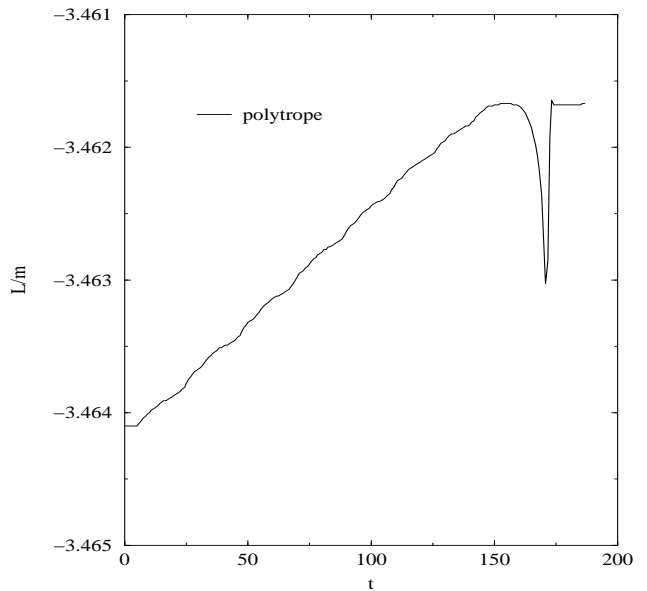


FIG. 6: Angular momentum per unit particle mass for the capture of a particle (polytropic model) by a black hole.

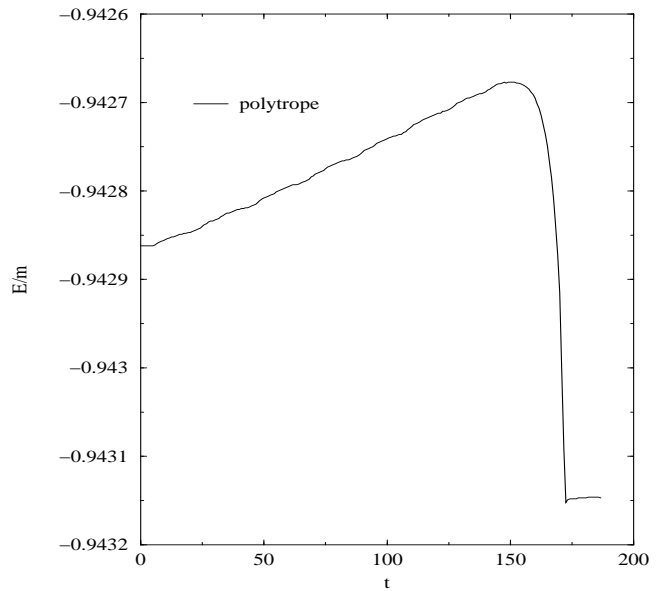


FIG. 7: Energy per unit particle mass for the capture of a particle (polytropic model) by a black hole.

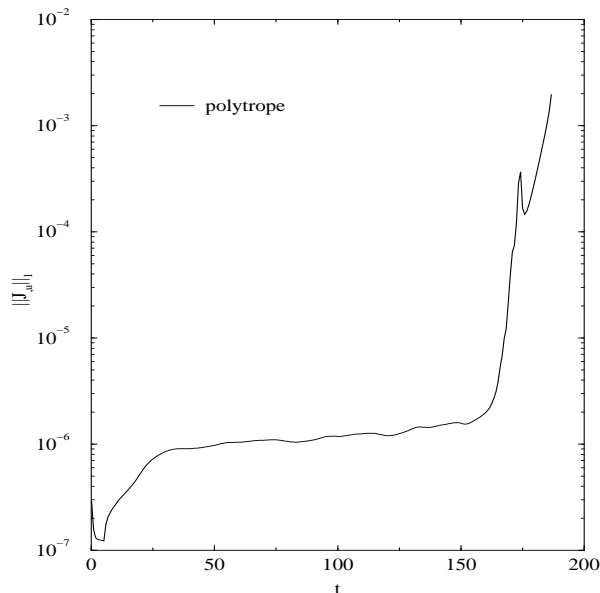


FIG. 8: L_1 norm of the radiation indicator, $\|J_{,u}\|_1$, shown using a logarithmic scale in the vertical axis, for the capture of a particle (polytropic model) by a black hole.

F. Speed of the code

The tests were performed on a Linux machine with a single processor running at 1.8GHz. One complete orbit run on a grid of $121 \times 2 \times 35^2$ points takes 21,000 time steps. The run time is about 20 hours. Of course, the run time scales with grid discretization as Δ^4 .

VI. CONCLUSION

The paper has described and implemented a particle method for evolving the full Einstein equations using a characteristic evolution code. The method can be expected to be a useful tool in modeling astrophysical situations involving a black hole and another much smaller object. We have demonstrated that the method works in the sense that it computes orbits that are qualitatively reasonable. Two models of a particle were investigated. The polytropic model gives better results in terms of smoothness of the computed motion and exhibited convergence. An important feature of the code is that it is much faster than other codes in which the material object is modeled using relativistic hydrodynamics.

Future work, as detailed below, is envisaged

- The gravitational radiation output (Bondi news function) is required, both to supply a waveform and to check the energy balance (the rate of loss of orbital energy mv_u should be of the same magnitude as the radiation power).

- The δ -function model has the advantage of simplicity. It offers a physically attractive way to model the motion and exterior gravitational field of an object of sufficiently small mass that its Schwarzschild radius cannot be resolved on the grid. The runs with this model do not crash but the lack of convergence checks on the evolution variables makes it problematic for making physical predictions. Perhaps the errors that arise in estimating the derivative of a function which is essentially singular can be better avoided by a more sophisticated integral approach akin to finite element methods. It is possible that such a treatment might lead to convergence of global quantities such as the radiated power.
- The prospects for obtaining reliable physical results with the polytropic model hinge upon several issues:

1. The errors inherent in the model, which were discussed qualitatively in Sec. III B, need to be sharpened to quantitative estimates.
2. Convergence testing is needed for runs over a significant time period and with physically realistic parameters.
3. We need to understand the effect of the polytrope radius (R_*) on the results. There should be some sense in which the particle motion is independent of R_* . Of course, taking the limit $R_* \rightarrow 0$ is equivalent to changing from the polytropic to the δ -function model, and this link provides further motivation for the continued investigation of the δ -function model.

In summary, the particle method has the potential to supply validated orbits, including inspirals towards the ISCO and plunges to the black hole, as well as the associated gravitational radiation output.

Acknowledgments

We benefited from the hospitality of the Max-Planck-Institut für GravitationsPhysik, Albert-Einstein-Institut and the Center for Gravitational Wave Physics at Pennsylvania State University (funded by the NSF cooperative agreement PHY-0114375). The work was supported by the National Research Foundation, South Africa under Grant number 2053724, and by NSF Grants PHY-9988663 to the University of Pittsburgh and PHY-0135390 to Carnegie Mellon University. We thank Manuela Campanelli and Carlos Lousto for discussions.

APPENDIX A: THE GEODESIC EQUATION

We have used Maple to compute the form of Eq. (4.1) for the metric (2.1). The formulas are given for the general case; and the formulas when the background option

is being used (see section III D) are obtained by setting the *undifferentiated* metric variables J , β , U to 0 and setting W to W_{an} . In the formulas, the angular part of v_i , v_A is represented by the spin weighted quantity $V_{\text{ang}} = v_{Aq}^A$. Further, for ease of application to the

approximate conservation formulas (sections III C and IV D), the formulas are presented with the background quantities (in each case, the first line) shown separately from the perturbative (E_i) quantities. The formulas are

$$\begin{aligned} \frac{dv_r}{d\tau} = & \frac{2\bar{V}_{\text{ang}}V_{\text{ang}} - v_r^2(rW_{,r} - W)r}{2r^3} \\ & + \left(4\bar{V}_{\text{ang}}V_{\text{ang}}(1 - K) - 2(e^{-2\beta} - 1)v_r^2(rW_{,r} - W)rK - 2J\bar{V}_{\text{ang}}^2K + 4\bar{V}_{\text{ang}}V_{\text{ang}}\bar{J}J - r\bar{V}_{\text{ang}}V_{\text{ang}}J_{,r}\bar{J} \right. \\ & - r\bar{V}_{\text{ang}}V_{\text{ang}}J\bar{J}_{,r} - 4\beta_{,r}e^{-2\beta}v_r r^3\bar{U}V_{\text{ang}}K - 4\beta_{,r}e^{-2\beta}v_r r^3U\bar{V}_{\text{ang}}K - 2J\bar{V}_{\text{ang}}^2K \\ & + 4e^{-2\beta}v_r^2\beta_{,r}(r + W)r^2K - 8\beta_{,r}e^{-2\beta}v_r r^3v_uK + rJ_{,r}\bar{V}_{\text{ang}}^2K + 2e^{-2\beta}v_r r^3\bar{U}_{,r}V_{\text{ang}}K \\ & \left. + 2e^{-2\beta}v_r r^3U_{,r}\bar{V}_{\text{ang}}K + r\bar{J}_{,r}V_{\text{ang}}^2K \right) \frac{1}{4Kr^3}; \end{aligned} \quad (\text{A1})$$

$$\begin{aligned} \frac{dV_{\text{ang}}}{d\tau} = & - \frac{(q + ip)\bar{V}_{\text{ang}}V_{\text{ang}}}{r^2} \\ & + \left(-4(q + ip)\bar{V}_{\text{ang}}V_{\text{ang}}(K - 1) + 4(\bar{\partial}K)J\bar{J}\bar{V}_{\text{ang}}V_{\text{ang}} - 2(\bar{\partial}J)K\bar{J}\bar{V}_{\text{ang}}V_{\text{ang}} - 2(\bar{\partial}\bar{J})K\bar{J}\bar{V}_{\text{ang}}V_{\text{ang}} \right. \\ & - 4e^{-2\beta}v_r(\bar{\partial}\beta)r^2U\bar{V}_{\text{ang}} - 4e^{-2\beta}v_r(\bar{\partial}\beta)r^2\bar{U}V_{\text{ang}} - 2e^{-2\beta}v_r^2(\bar{\partial}W)r + 4e^{-2\beta}v_r^2(r + W)(\bar{\partial}\beta)r \\ & - 8e^{-2\beta}v_r(\bar{\partial}\beta)r^2v_u + (\bar{\partial}\bar{J})J^2\bar{V}_{\text{ang}}^2 + (\bar{\partial}J)\bar{J}^2V_{\text{ang}}^2 - 2(\bar{\partial}K)JK\bar{V}_{\text{ang}}^2 - 2(\bar{\partial}K)\bar{J}KV_{\text{ang}}^2 + 2(\bar{\partial}K)\bar{V}_{\text{ang}}V_{\text{ang}} \\ & + (\bar{\partial}J)\bar{V}_{\text{ang}}^2\bar{J}J + (\bar{\partial}\bar{J})V_{\text{ang}}^2\bar{J}J + 4ip\bar{J}V_{\text{ang}}^2 + (\bar{\partial}J)\bar{V}_{\text{ang}}^2 + (\bar{\partial}\bar{J})V_{\text{ang}}^2 + 4q\bar{J}V_{\text{ang}}^2 + 2r^2e^{-2\beta}v_r(\bar{\partial}\bar{U})V_{\text{ang}} \\ & \left. + 2r^2e^{-2\beta}v_r(\bar{\partial}U)\bar{V}_{\text{ang}} + 4r^2e^{-2\beta}v_rq\bar{U}V_{\text{ang}} + 4ir^2e^{-2\beta}v_r p\bar{U}V_{\text{ang}} \right) \frac{1}{4r^2}. \end{aligned} \quad (\text{A2})$$

-
- [1] L. Blanchet, G. Faye, B. R. Iyer, and B. Joguet, Phys. Rev. D **65**, 061501 (2002).
- [2] L. Gualtieri, E. Berti, J. A. Pons, G. Miniutti, and V. Ferrari, Phys. Rev. D **64**, 104007 (2001).
- [3] L. Barack, Y. Mino, H. Nakano, A. Ori, and M. Sasaki, Phys. Rev. Lett. **88**, 091101 (2002).
- [4] M. J. Pfenning and E. Poisson, Phys. Rev. D **65**, 084001 (2002).
- [5] L. Barack and C. O. Lousto, Phys. Rev. D **66**, 061502 (2002).
- [6] C. O. Lousto, Class. Quant. Grav. **18**, 3989 (2001).
- [7] T. C. Quinn and R. M. Wald, Phys. Rev. D **56**, 3381 (1997).
- [8] Y. Mino, M. Sasaki, and T. Tanaka, Prog. Theor. Phys. Suppl. **128**, 373 (1997).
- [9] K. Glampedakis, S. A. Hughes, and D. Kennefick, Phys. Rev. D **66**, 064005 (2002).
- [10] P. Papadopoulos and J. A. Font, Phys. Rev. D **61**, 024015 (2000).
- [11] M. Shibata and K. Uryu, Phys. Rev. D **64**, 104017 (2001).
- [12] E. Gourgoulhon, P. Grandclément, K. Taniguchi, J.-A. Marck, and S. Bonazzola, Phys. Rev. D **63**, 064029 (2001).
- [13] J. A. Faber and F. A. Rasio, Phys. Rev. D **63**, 044012 (2001).
- [14] K. Oohara and T. Nakamura, Prog. Theor. Phys. **136**, 270 (1999).
- [15] J. Font, T. Goodale, S. Iyer, M. M. L. Rezzolla, E. Seidel, N. Stergioulas, W. Suen, and M. Tobias, Phys. Rev. D **65**, 084024 (2002).
- [16] M. Shibata and K. Uryu, in *Proceedings of the 16th International Conference on General Relativity & Gravitation*, edited by N. T. Bishop and S. D. Maharaj (World Scientific, Singapore, 2002).
- [17] L. S. Finn and K. S. Thorne, Phys. Rev. D **62**, 124021 (2000).
- [18] N. T. Bishop, R. Gómez, L. Lehner, M. Maharaj, and J. Winicour, Phys. Rev. D **56**, 6298 (1997).
- [19] R. Gómez, Phys. Rev. D **64**, 024007 (2001).
- [20] N. T. Bishop, R. Gómez, L. Lehner, and J. Winicour, Phys. Rev. D **54**, 6153 (1996).
- [21] R. A. Isaacson, J. S. Welling, and J. Winicour, J. Math. Phys. **26**, 2859 (1985).
- [22] N. T. Bishop, Class. Quantum Grav. **10**, 333 (1993).
- [23] N. T. Bishop, C. J. S. Clarke, and R. A. d'Inverno, Class. Quantum Grav. **7**, L23 (1993).
- [24] R. A. Isaacson, J. S. Welling, and J. Winicour, J. Math. Phys. **24**, 1824 (1983).

- [25] H. Bondi, M. J. G. van der Burg, and A. W. K. Metzner, Proc. R. Soc. London **A269**, 21 (1962).
- [26] L. A. Tamburino and J. Winicour, Phys. Rev. **150**, 1039 (1966).
- [27] R. K. Sachs, Proc. R. Soc. London **A270**, 103 (1962).
- [28] R. Gómez, L. Lehner, P. Papadopoulos, and J. Winicour, Class. Quantum Grav. **14**, 977 (1997).
- [29] N. T. Bishop, R. Gómez, L. Lehner, M. Maharaj, and J. Winicour, Phys. Rev. D **60**, 024005 (1999).
- [30] S. Chandrasekhar, *An introduction to the study of stellar structure* (Dover, New York, 1967).
- [31] J. Winicour, J. Math. Phys. **24**, 1193 (1983).
- [32] J. Winicour, J. Math. Phys. **24**, 2056 (1983).
- [33] Y. E. Zlochower, Ph.D. thesis, University of Pittsburgh (2002).